Appendix K: Additional Polar/CAMMICE/MICS Plots

K.1 Niehof H^+ observations in aggregate

In this subsection we include additional figures similar to the four presented earlier in Section 3.4.1. These figures include mean pitch angle distributions, spectra, energy-*L* spectrograms, and equatorial maps computed from aggregating the Niehof data set in the same way as described above.

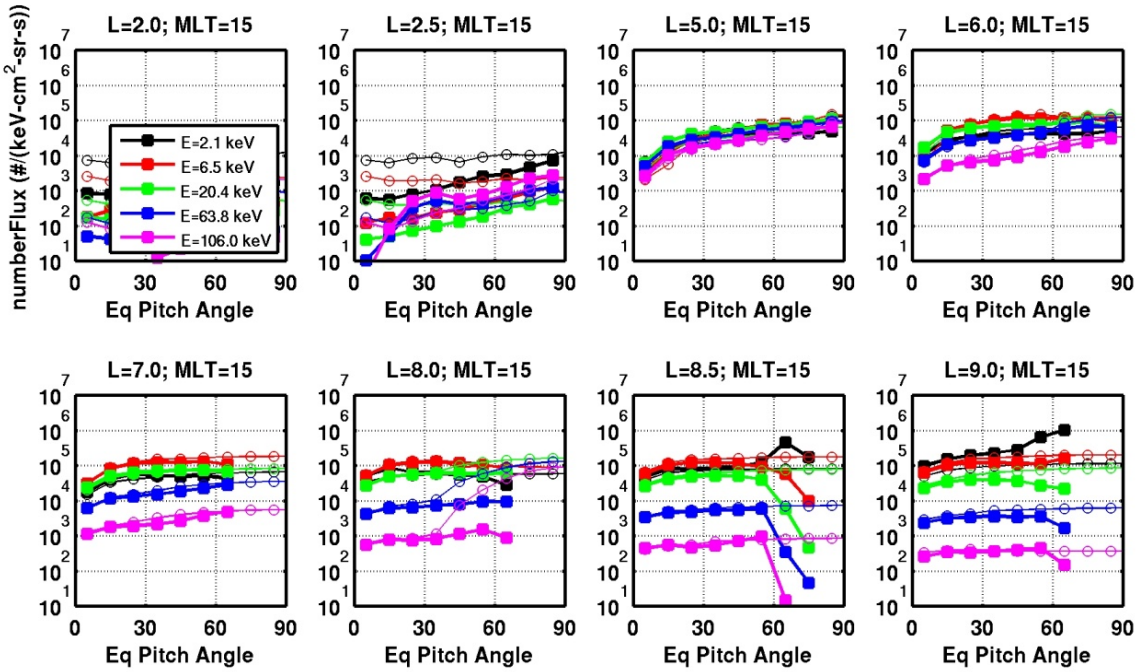

Figure 164. Mean H^+ pitch angle distributions aggregated from the Niehof files (thick lines) and Roeder's 2005 database (thin lines).

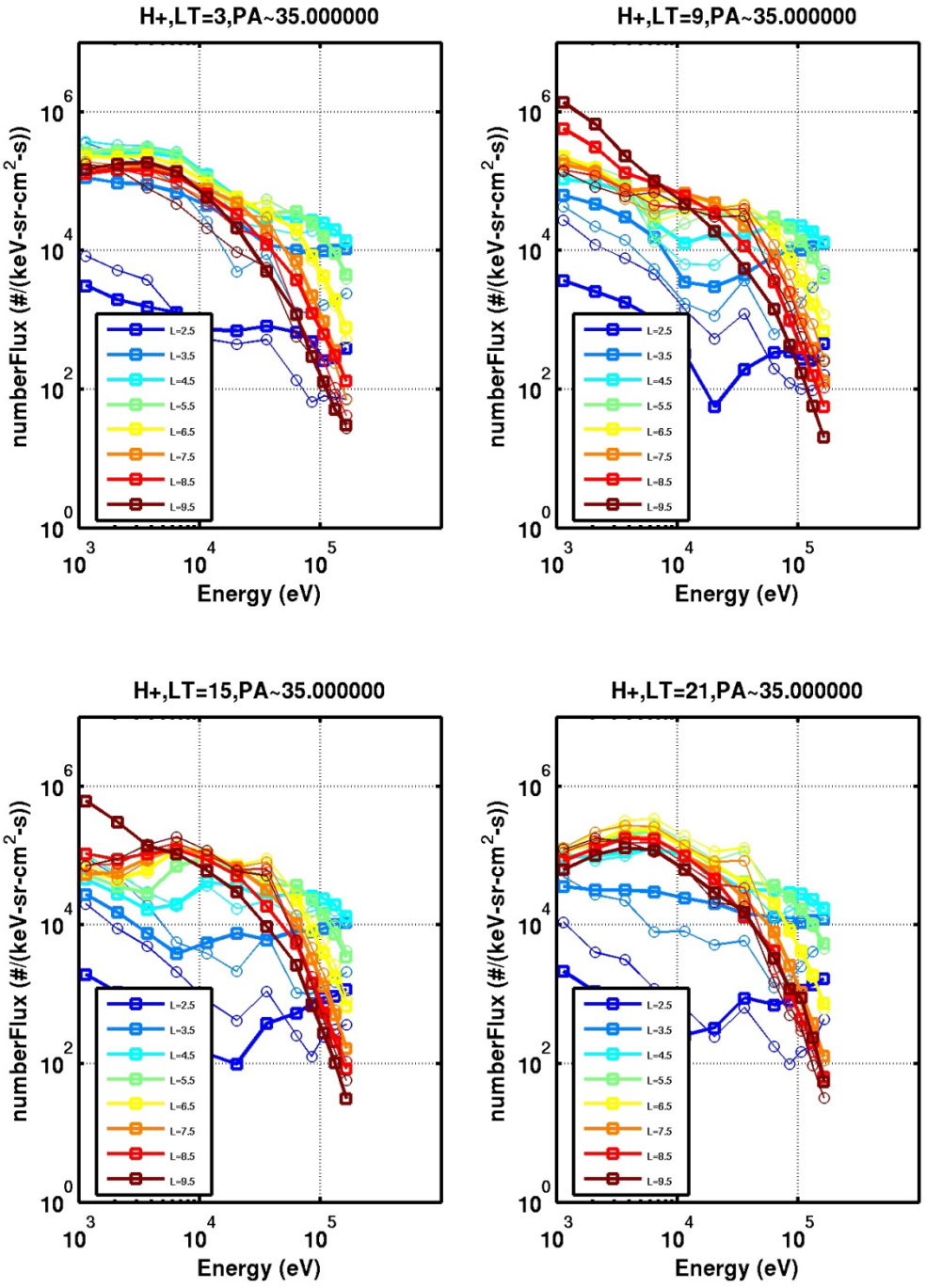

Figure 165. Mean H^+ spectra aggregated from the Niehof files (thick lines) and Roeder's 2005 database (thin lines).

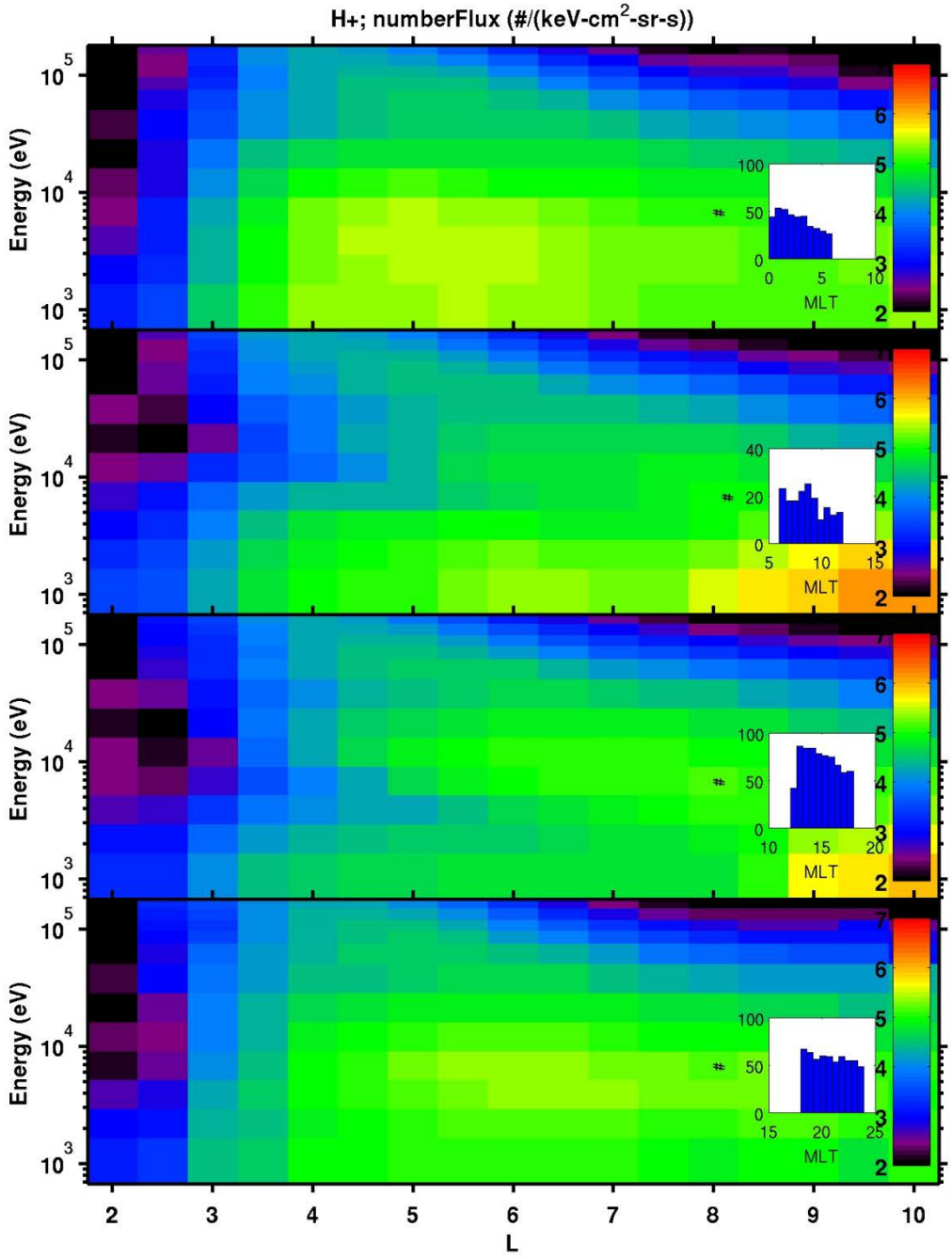

Figure 166. Mean H^+ fluxes binned from the Niehof files plotted by energy and *L*.

K.2 Roeder He^+ observations in aggregate

In this subsection we include additional figures similar to the four presented earlier in Section 3.4.1, but from the Roeder data set and for He^+. These figures include mean pitch angle distributions, spectra, energy-*L* spectrograms, and equatorial maps computed from aggregating the Roeder data set in the same way as described above.

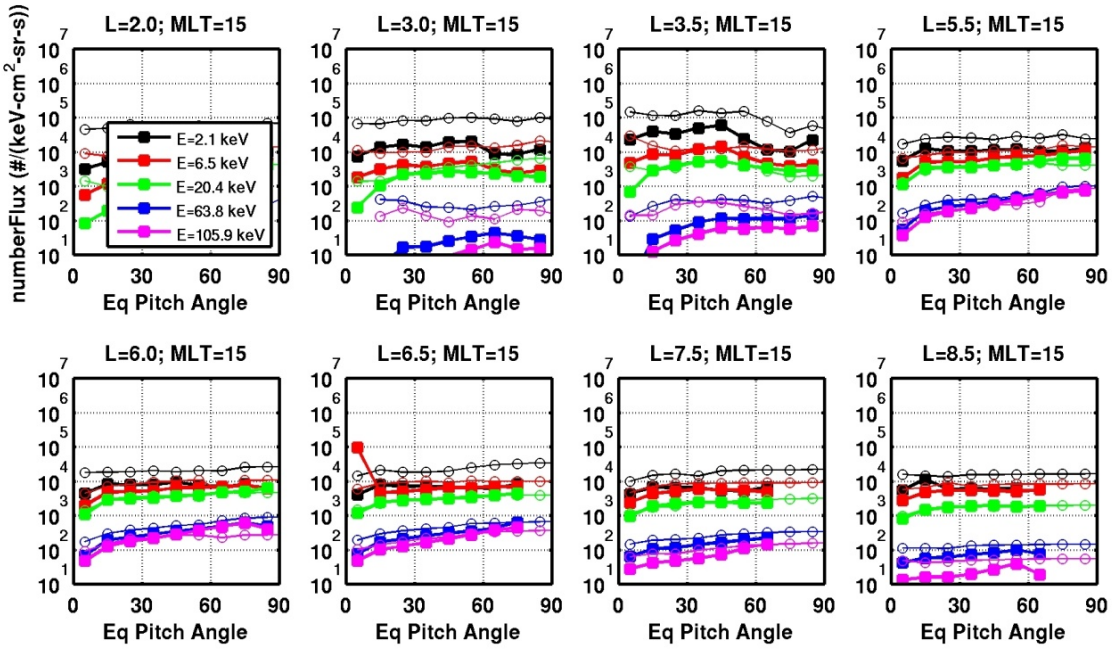

Figure 167. Mean He^+ pitch angle distributions aggregated from the Niehof files (thick lines) and Roeder's 2005 database (thin lines).

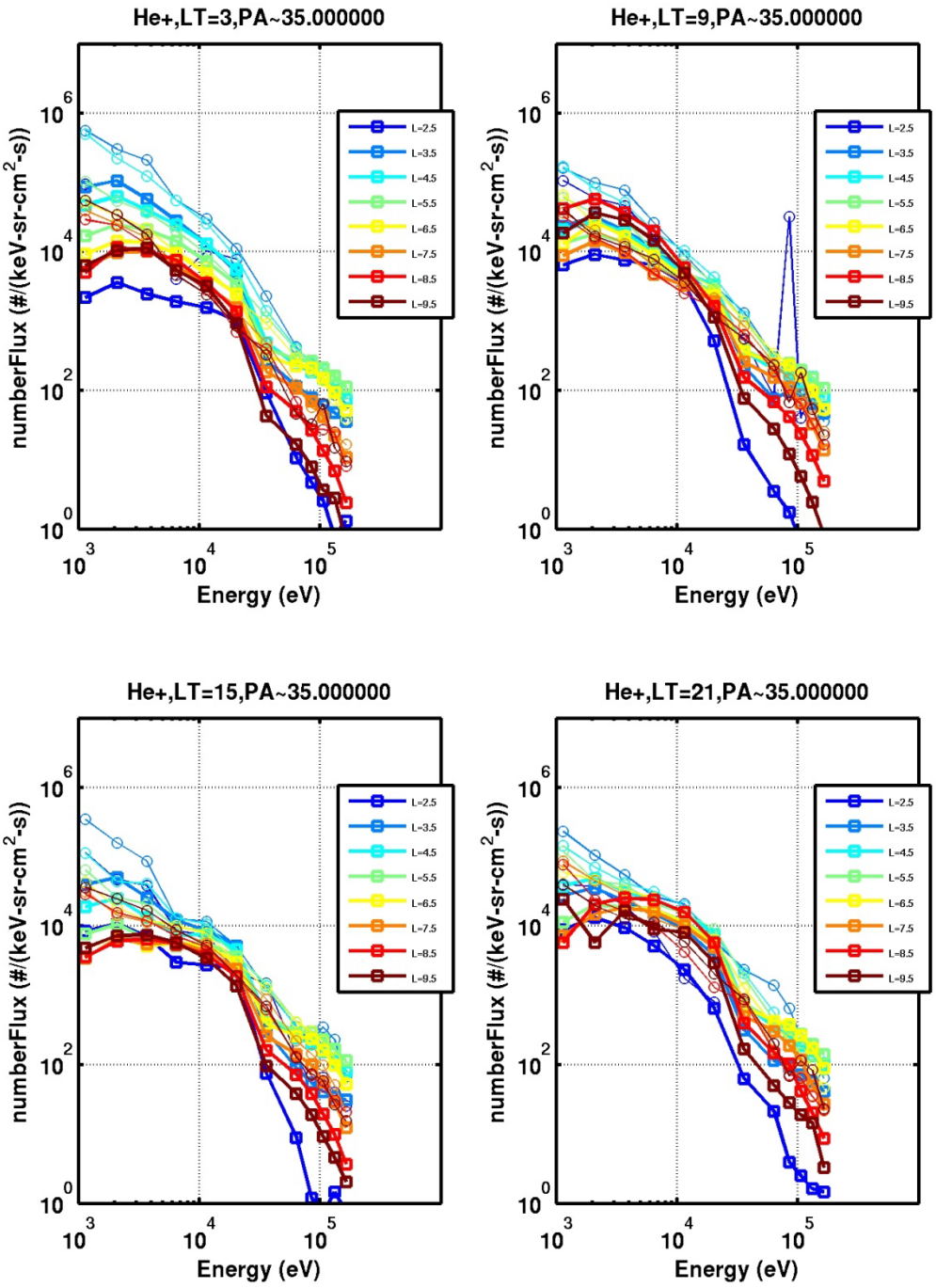

Figure 168. Mean He^+ spectra aggregated from the Niehof files (thick lines) and Roeder's 2005 database (thin lines).

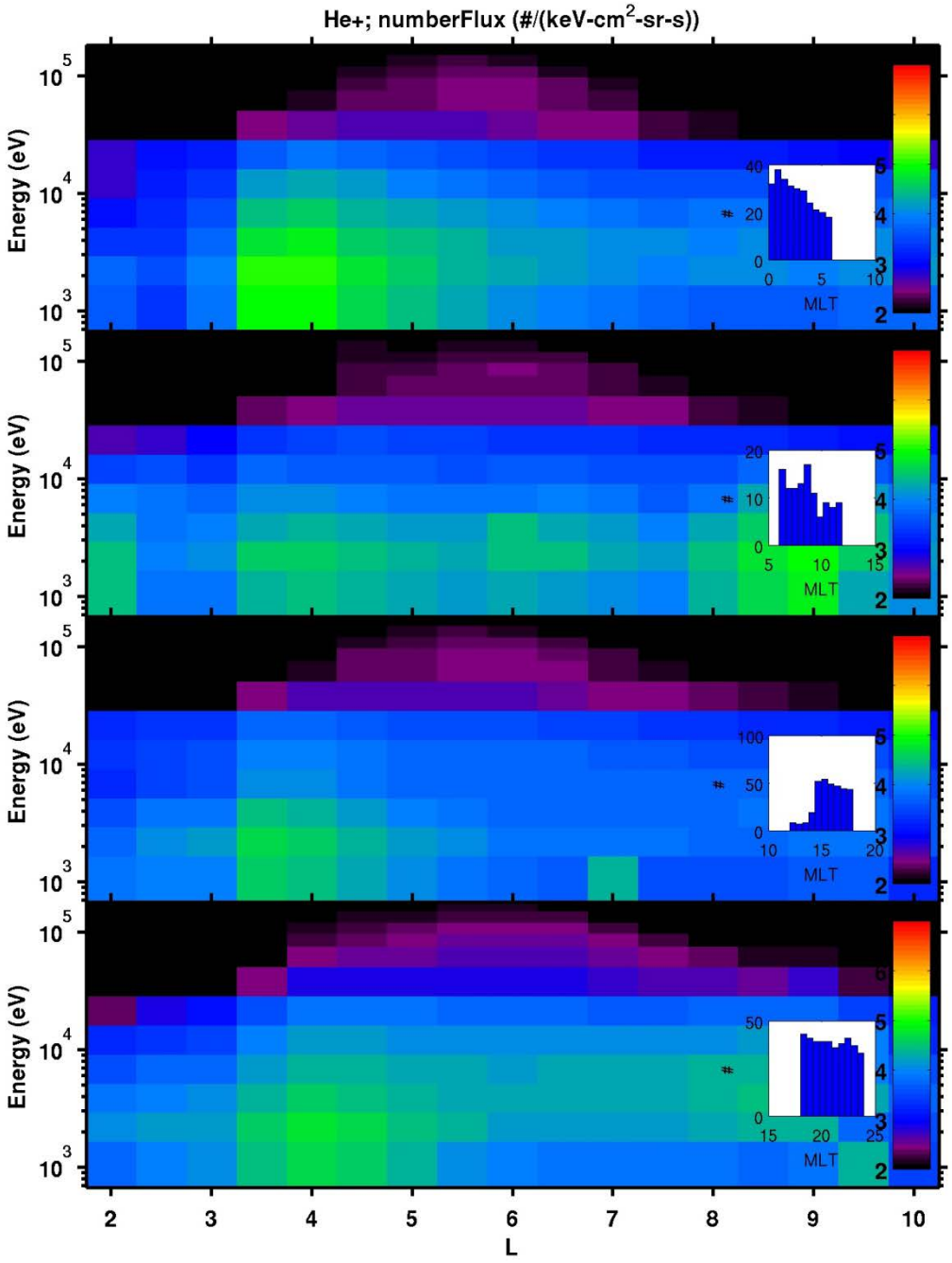

Figure 169. Mean He^+ fluxes binned from the Roeder files plotted by energy and *L*.

K.3 Niehof He^+ observations in aggregate

In this subsection we include additional figures similar to the four presented earlier in Section 3.4.1 derived from the Niehof data set of He^+ fluxes. These figures include mean pitch angle distributions, spectra, energy-*L* spectrograms, and equatorial maps computed from aggregating the Niehof data set in the same way as described above.

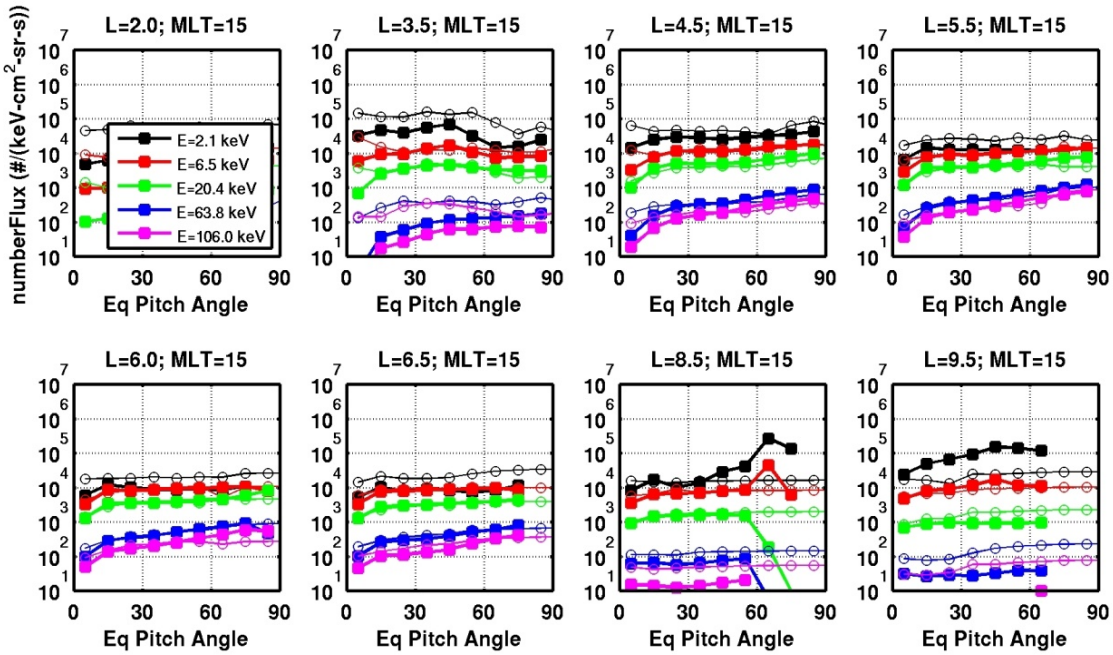

Figure 170. Mean He^+ pitch angle distributions aggregated from the Roeder files (thick lines) and Roeder's 2005 database (thin lines).

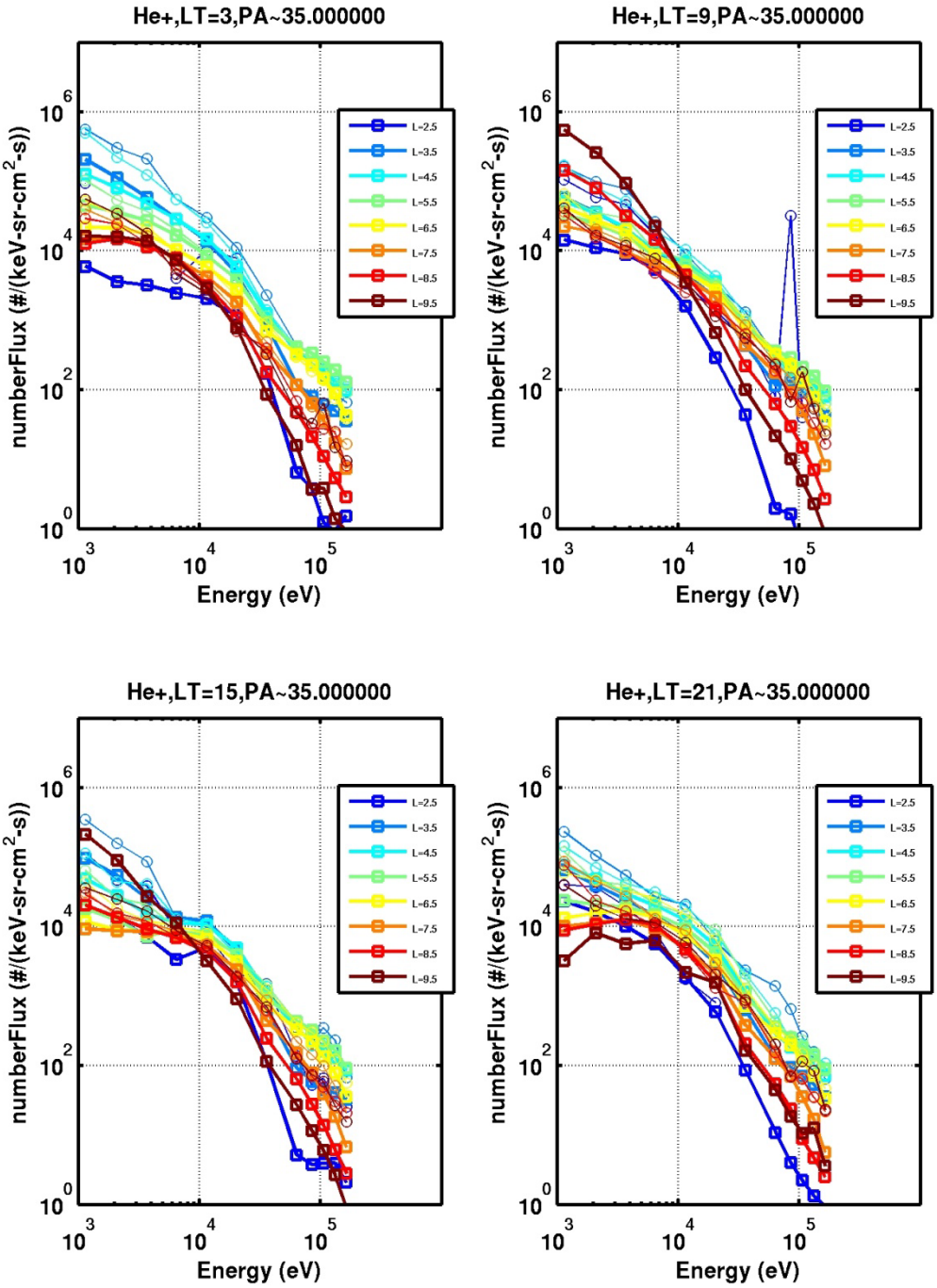

Figure 171. Mean He^+ spectra aggregated from the Niehof files (thick lines) and Roeder's 2005 database (thin lines).

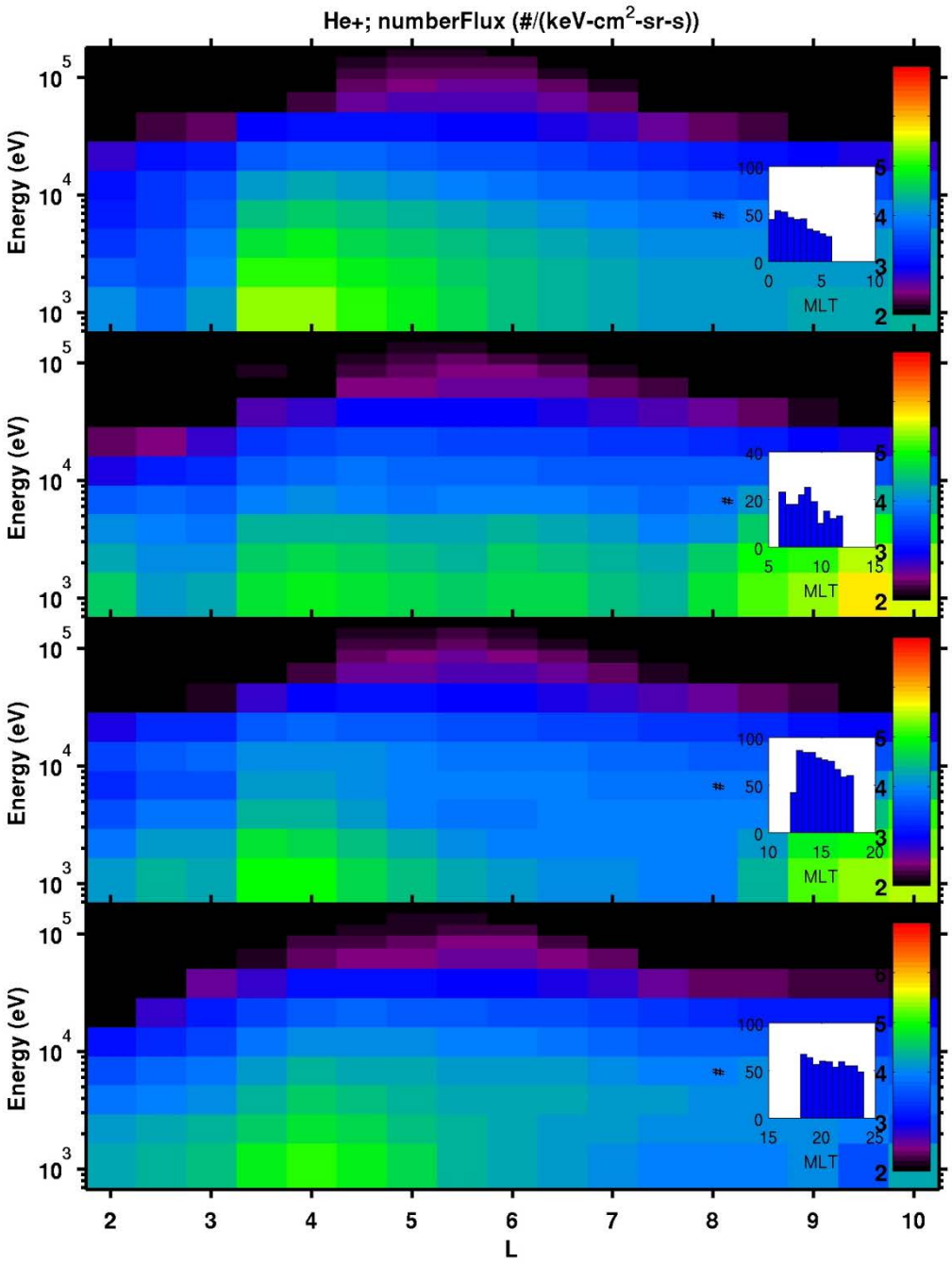

Figure 172. Mean He^+ fluxes binned from the Niehof files plotted by energy and *L*.

K.4 Roeder O^+ observations in aggregate

In this subsection we include additional figures similar to the four presented earlier in Section 3.4.1. These figures include mean pitch angle distributions, spectra, energy-*L* spectrograms, and equatorial maps computed from aggregating the Roeder data set in the same way as described above.

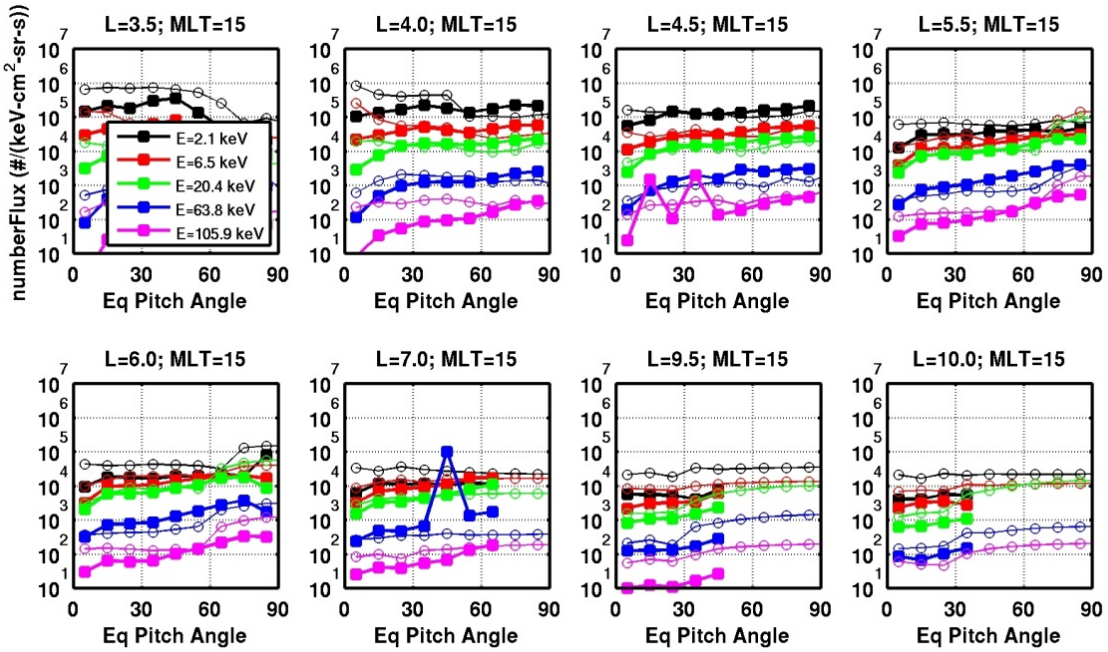

Figure 173. Mean O^+ pitch angle distributions aggregated from the Roeder files (thick lines) and Roeder's 2005 database (thin lines).

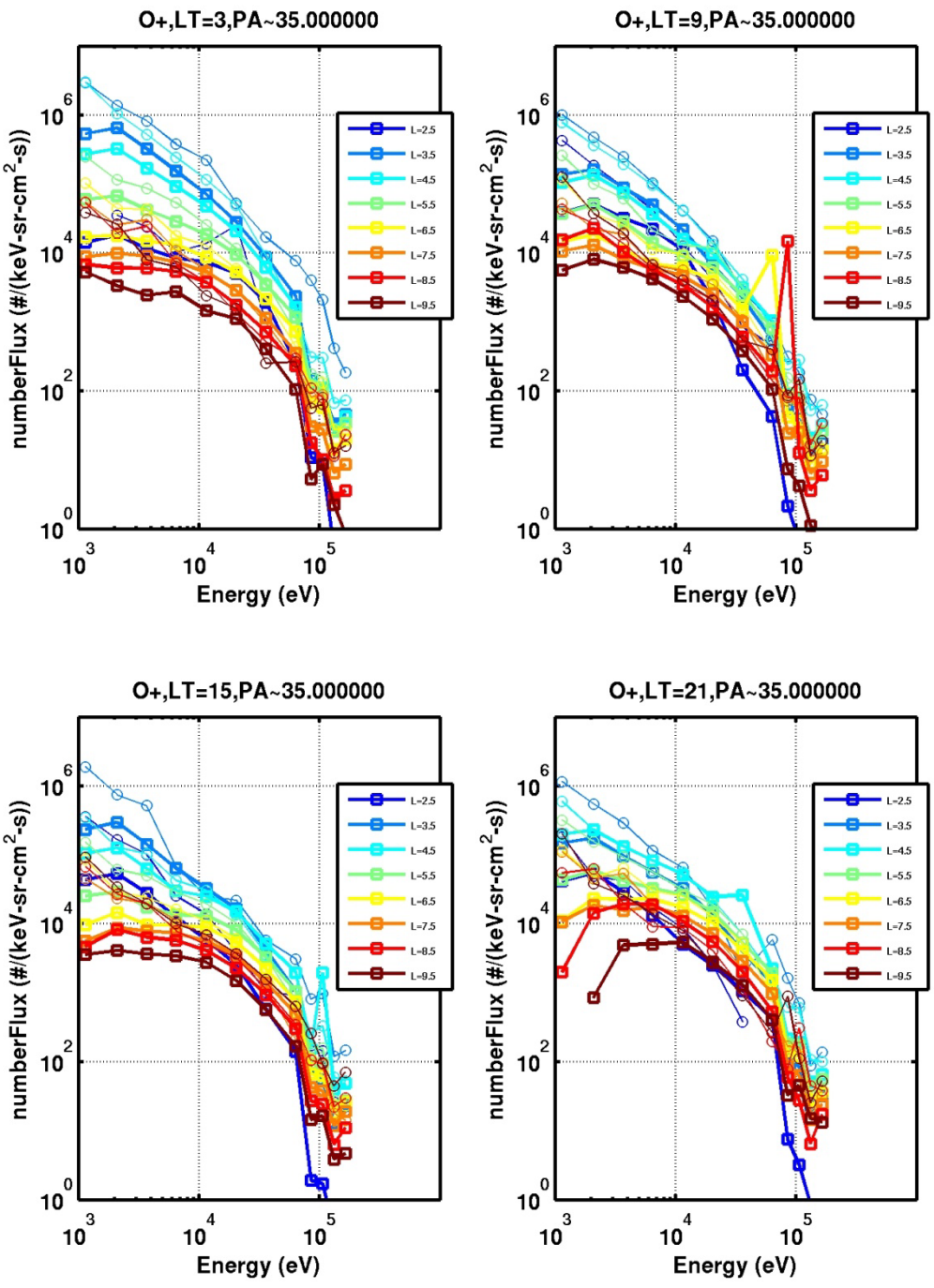

Figure 174. Mean O^+ spectra aggregated from the Roeder files (thick lines) and Roeder's 2005 database (thin lines).

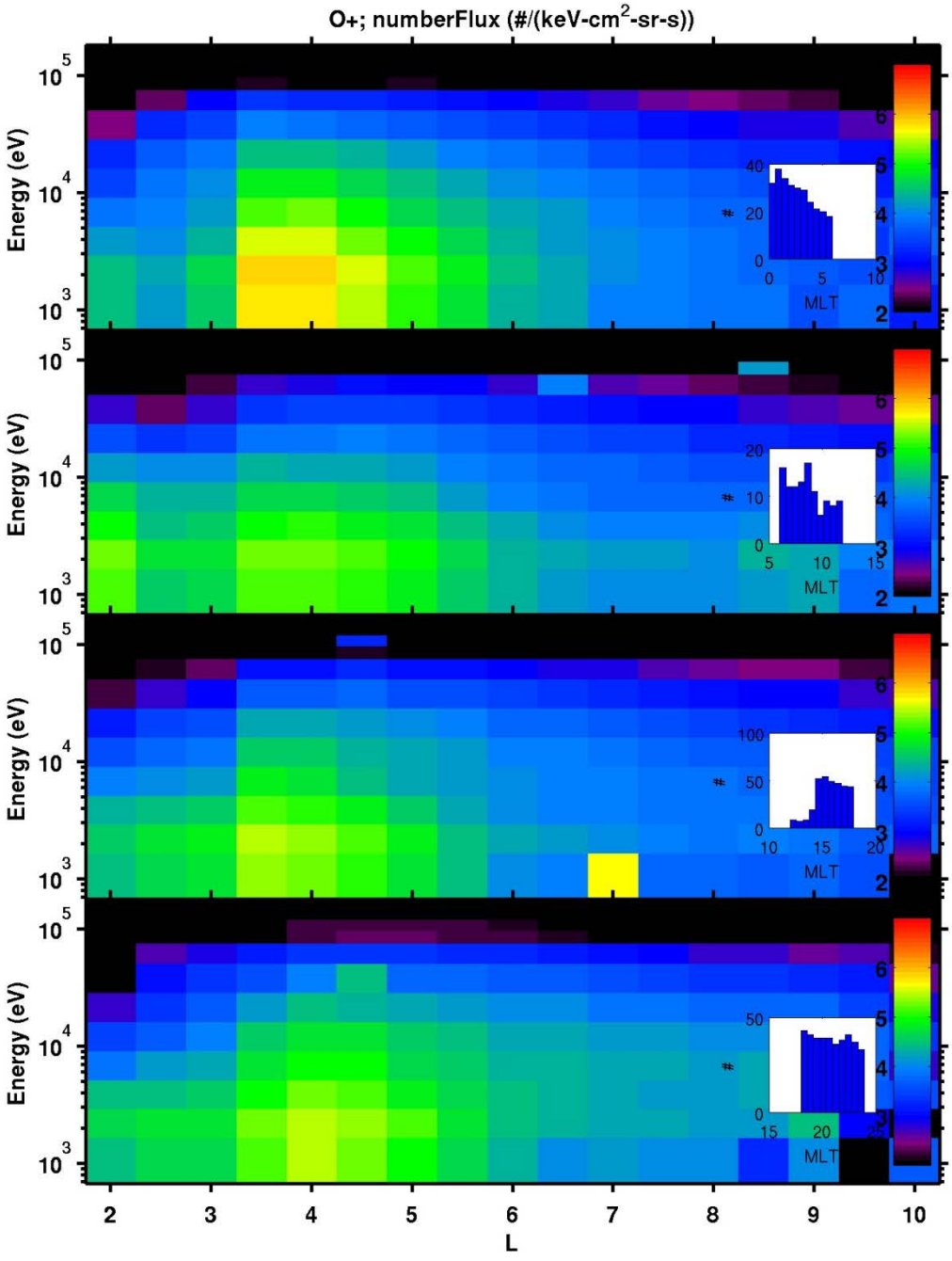

Figure 175. Mean O^+ fluxes binned from the Roeder files plotted by energy and *L*.

K.5 Niehof O^+ observations in aggregate

In this subsection we include additional figures similar to the four presented earlier in Section 3.4.1. These figures include mean pitch angle distributions, spectra, energy-*L* spectrograms, and equatorial maps computed from aggregating the Niehof data set in the same way as described above.

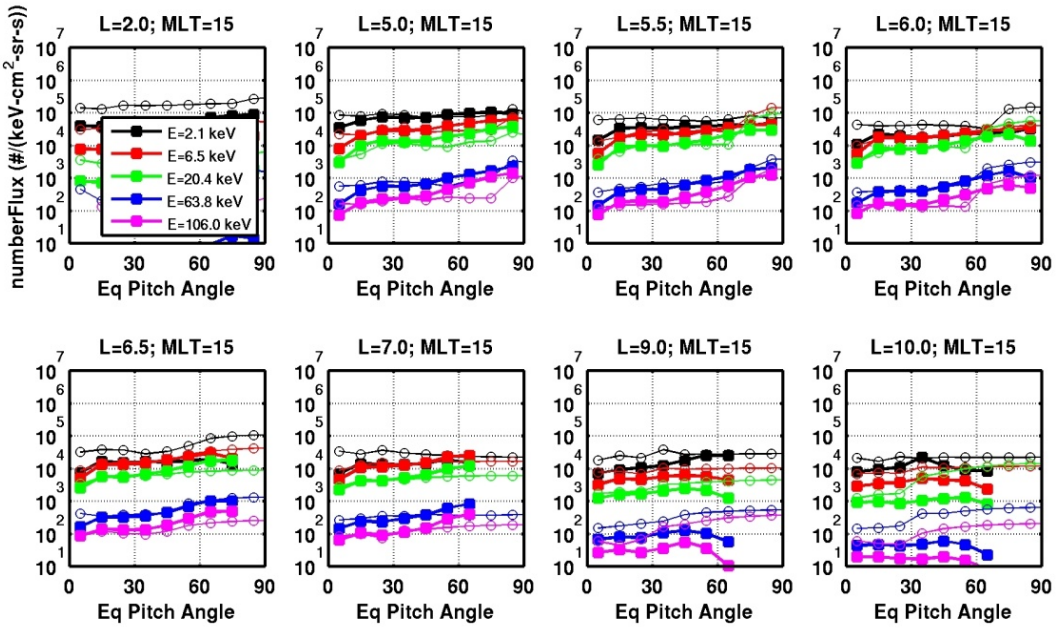

Figure 176. Mean O^+ pitch angle distributions aggregated from the Niehof files (thick lines) and Roeder's 2005 database (thin lines).

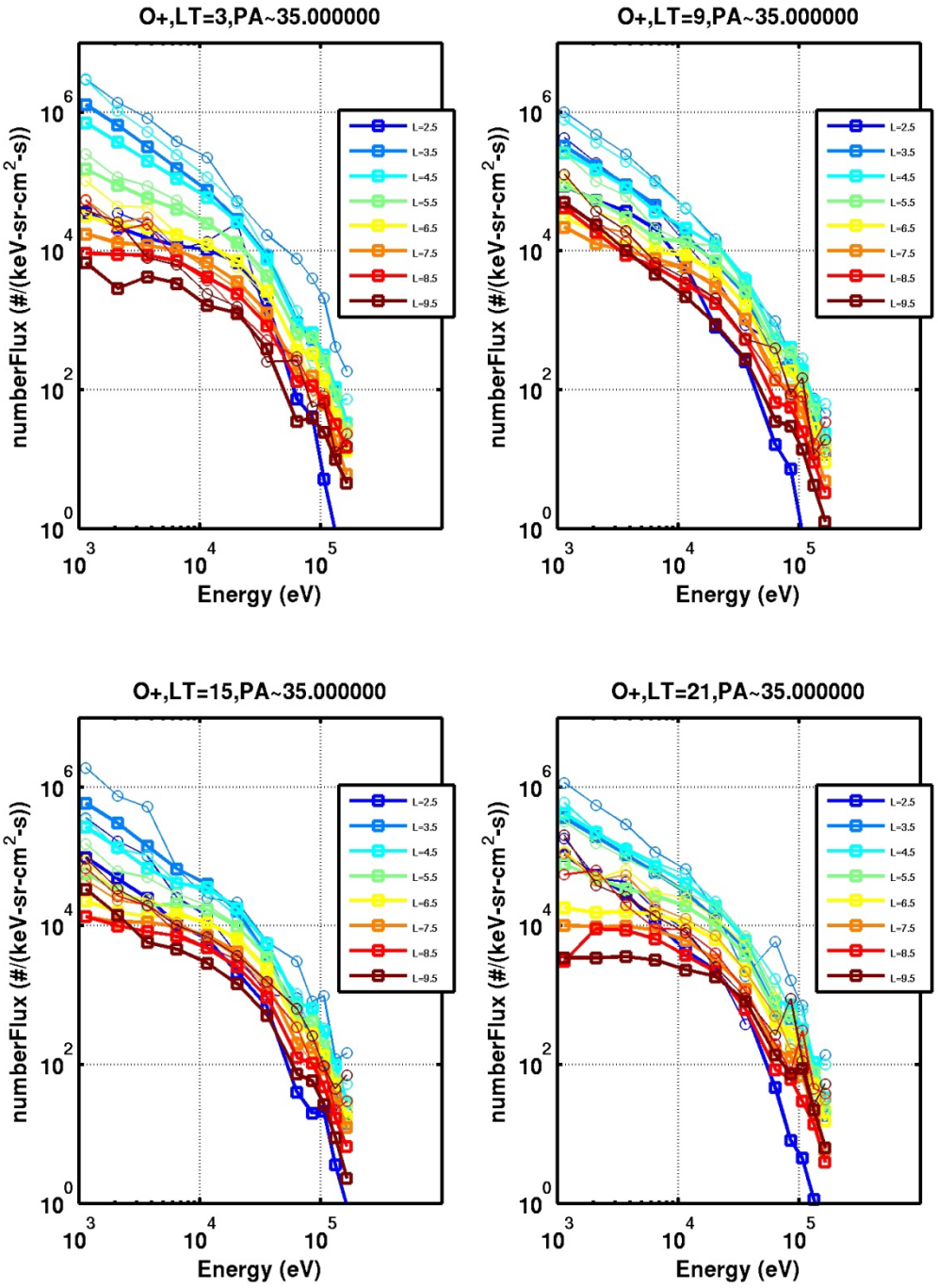

Figure 177. Mean O^+ spectra aggregated from the Niehof files (thick lines) and Roeder's 2005 database (thin lines).

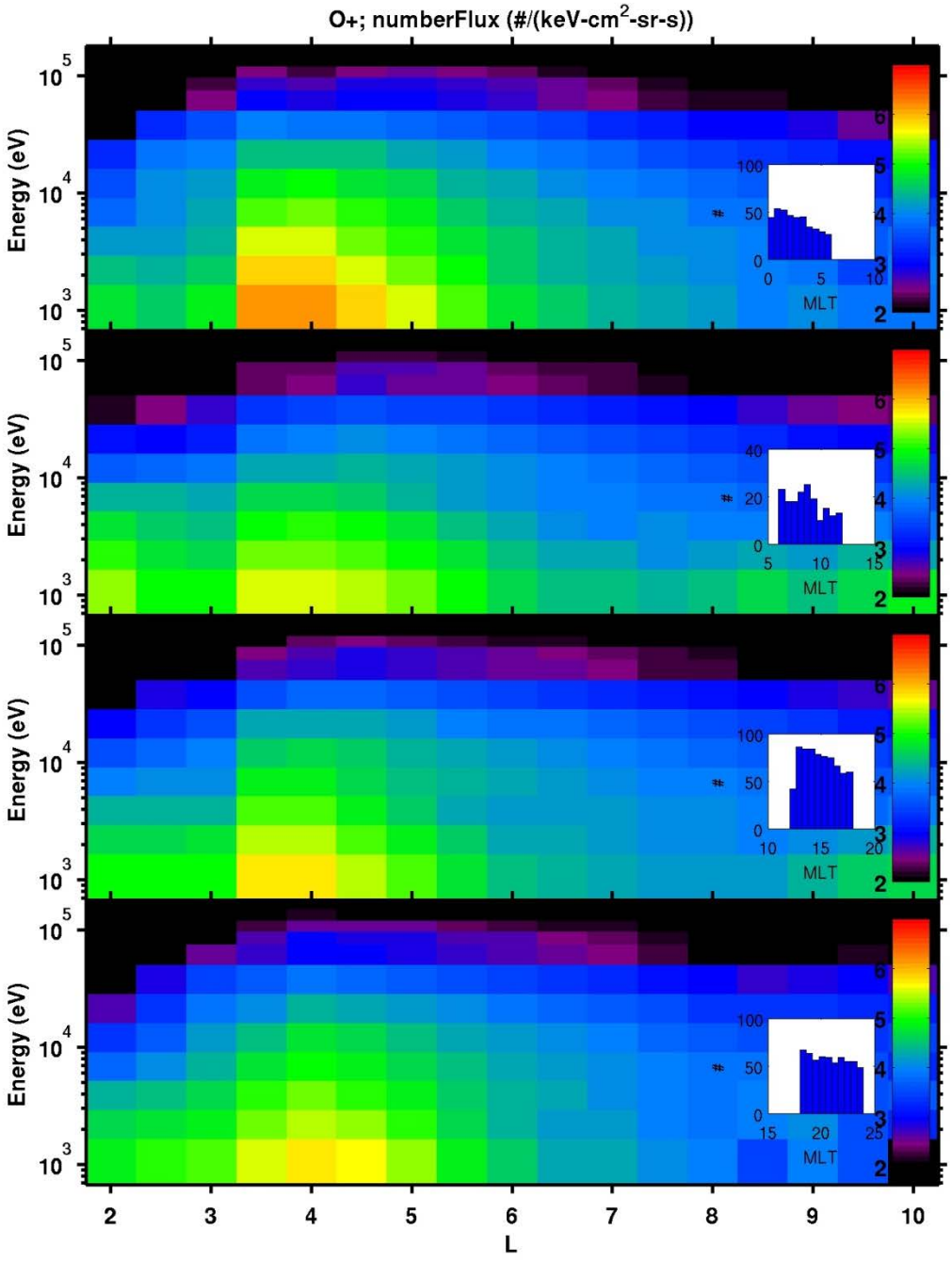

Figure 178. Mean O^+ fluxes binned from the Niehof files plotted by energy and *L*.